Formation of NaCl-Type Monodeuteride LaD by the Disproportionation Reaction of LaD_2

A. Machida,[1,*] M. Honda,[2,†] T. Hattori,[2,3] A. Sano-Furukawa,[2,3] T. Watanuki,[1] Y. Katayama,[1] K. Aoki,[1,‡] K. Komatsu,[4] H. Arima,[3,‡] H. Ohshita,[5] K. Ikeda,[5] K. Suzuya,[3] T. Otomo,[5] M. Tsubota,[6,§] K. Doi,[6] T. Ichikawa,[6] Y. Kojima,[6] and D. Y. Kim[7,8]

[1]*Quantum Beam Science Directorate, Japan Atomic Energy Agency, Hyogo 679-5148, Japan*
[2]*Quantum Beam Science Directorate, Japan Atomic Energy Agency, Ibaraki 319-1195, Japan*
[3]*J-PARC Center, Japan Atomic Energy Agency, Ibaraki 319-1195, Japan*
[4]*Geochemical Research Center, Graduate School of Science, University of Tokyo, Tokyo 113-0033, Japan*
[5]*Institute of Materials Structure Science, High Energy Accelerator Research Organization (KEK), Ibaraki 305-0801, Japan*
[6]*Institute for Advanced Materials Research, Hiroshima University, Hiroshima 739-8530, Japan*
[7]*Theory of Condensed Matter Group, Cavendish Laboratory, University of Cambridge, Cambridge CB3 0HE, United Kingdom*
[8]*Geophysical Laboratory, Carnegie Institution of Washington, Washington D.C. 20015, USA*

(Received 18 August 2011; revised manuscript received 13 March 2012; published 14 May 2012)

Previous x-ray diffraction measurements revealed the pressure-induced decomposition of an fcc $LaH_{2.3}$ into H-rich and H-poor fcc phases around 11 GPa. The present neutron diffraction measurements on LaD_2 confirm the formation of NaCl-type LaD as a counterpart of the D-rich $LaD_{2+\delta}$ by disproportionation. First-principles enthalpy and lattice dynamic calculations demonstrate that the NaCl-type LaH is stabilized at high pressures and can be recovered at ambient conditions. Finding the NaCl-type LaH will pave the way for investigations on the site-dependent nature of hydrogen-metal interactions.

DOI: 10.1103/PhysRevLett.108.205501 PACS numbers: 81.40.Vw, 61.05.F−, 62.50.−p, 63.20.D−

Rare-earth metals are easily hydrogenated upon exposure to H_2 gas [1]. H_2 molecules on a metal surface dissociate into H atoms, which diffuse into the metal lattice and occupy interstitial sites by forming hydrogen-metal (H-*M*) bonds. The amount of absorbed H is limited by the number of interstitial sites available for H. Typical hcp and fcc metal lattices have two tetrahedral interstitial (*T* site) and one octahedral interstitial (*O* site) sites per metal atom and, consequently, are capable of containing up to 75 at. % of H or forming trihydrides.

La, a prototype for rare-earth metals, forms both LaH_2 and LaH_3 in which H atoms are accommodated in only the *T* sites and both the *T* and *O* sites of the fcc metal lattice, respectively [2,3]. H atoms prefer to occupy the *T* sites rather than the *O* sites, and LaH_2 is formed during the early stage of hydrogenation. Further hydrogenation of LaH_2 or adding additional H atoms into the empty *O* sites causes a metal-insulator transition [4]. Hydrogenation-induced metal-insulator transition is commonly observed for rare-earth metals, and the H-*M* interactions at the *O* site play a key role in such electronic changes. However, the behavior of H in these rare-earth-metal hydrides seems still under debate [5–10]. Monohydride LaH with H atoms in only *O* sites would shed light on the *O*-site interactions and further the site-dependent nature of H-*M* bonds through a comparison study among mono-, di-, and trihydrides. Although the synthesis of fcc LaH has yet to be reported, the occupation of the *O* site has been theoretically predicted to be energetically favorable for fcc LaH_x in $x < 0.1$ [11].

Our previous synchrotron radiation (SR) x-ray diffraction (XRD) measurements revealed that dihydrides with fcc metal lattices commonly decompose into H-rich and H-poor fcc phases [12]. Ambient temperature compression of LaH_2 causes the metal lattice to distort from fcc to face-center-tetragonal (fct), and disproportionation occurs at 11 GPa. Infrared spectroscopy measurements indicate that the H-rich phase gradually approaches LaH_3 upon further compression [13]. Comparing the volume expansions of the metal lattices for the H-poor phase and pure La metal at corresponding pressures, the estimated H composition of the H-poor phase LaH_x is 0.6–0.7. This value is unusually large for a solid solution.

In this Letter, we present the unprecedented formation of monodeuteride (fcc LaD) with octahedrally coordinated deuterium by disproportionation reaction. The neutron powder diffraction (NPD) measurements on LaD_2 are performed to determine the location and occupancy of the D atoms in the fcc metal lattices. Additionally, a first-principles calculation reveals the thermodynamics underlining the disproportionation reaction.

For a synthesis of LaD_2, stoichiometrically weighted D_2 gas was introduced to react with the powder La metal at 400 °C for 8 hours. The NPD pattern taken at ambient conditions was indexed with a single phase of fcc LaD_2. Rietveld refinement of the NPD pattern using the Z-RIETVELD program [14] yielded a lattice constant 5.652 (2) Å and D occupancies of 0.94(4) and 0.09(6) for the *T* site and *O* site, respectively. The D concentration was 1.99 ± 0.15. These structural parameters agree well with previously reported values [15].

SR-XRD measurements were conducted for LaD_2 at pressures up to 18 GPa at ambient temperature using the

high-pressure station of BL22XU [16] at SPring-8. A diamond anvil cell was employed as a high-pressure cell. Details of the experimental setup and techniques are reported elsewhere [12,17].

A Paris-Edinburgh press [18] was employed for high-pressure NPD measurements. A metal gasket composed of a TiZr null alloy, the shape and size of which were optimized in advance by using SR x rays at BL14B1, SPring-8, was employed to generate high pressures above the disproportionation pressure in the Paris-Edinburgh cell. LaD_2 powder was encapsulated together with a pressure medium of a deuterated methanol-ethanol 4:1 mixture in the metal gasket and pressurized between the opposing double-toroidal anvils made of sintered diamonds. NPD patterns were measured up to 17 GPa at ambient temperature by using a high-intensity total diffractometer, NOVA, constructed at a pulsed neutron facility, J-PARC. The sample pressures were estimated from the equation of state determined for LaD_2 by the SR-XRD measurement. Simulated diffraction patterns were calculated by using the RIETAN-FP program [19]. Details of the experimental setup and techniques are reported elsewhere [20].

The calculations are based on the generalized gradient approximation [21] with the Perdew-Burke-Ernzerhof parameterization [22] for the exchange-correlation functional to density functional theory [23,24] using QUANTUM ESPRESSO code [25]. The electronic orbitals were expanded in a plane wave basis set with a kinetic energy cutoff of 60 Ry. The Brillouin zone integrations in the electronic calculations were performed by using the Monkhorst-Pack method [26] with a $24 \times 24 \times 24$ mesh. Phonon calculations were conducted with density functional perturbation theory [27] with a $8 \times 8 \times 8$ mesh.

Similar to $LaH_{2.3}$ [12], SR-XRD measurements indicate that LaD_2 decomposes into two deuterides at 11 GPa. The fcc metal lattice of LaD_2 initially distorts into an fct lattice upon compression and decomposes into fcc and fct metal lattices at 11 GPa. The molar-volume difference between the fcc and fct phases just after disproportionation is 4.86 cm^3/mol at 11.8 GPa for the deuteride and 4.73 cm^3/mol at 11.2 GPa for the hydride; these observations are within the experimental accuracy. The volume-pressure relations of LaD_2 and $LaH_{2.3}$ are fitted by almost identical equations of state in the pressure region up to the disproportionation pressure 11 GPa. Additionally, H-D substitution does not influence the disproportionation pressure or the compression curves. Although details of the XRD results for LaD_2 are not presented here, those for $LaH_{2.3}$ are reported in Ref. [12].

Figure 1 shows the NPD patterns of the starting material LaD_2 at pressures beyond the disproportionation pressure. All the diffraction peaks of the 2.7-GPa pattern are indexed with an fcc structure of LaD_2. Each peak shifts to a small d value as the pressure increases, indicating a gradual contraction of the metal lattice. The diffraction profile clearly

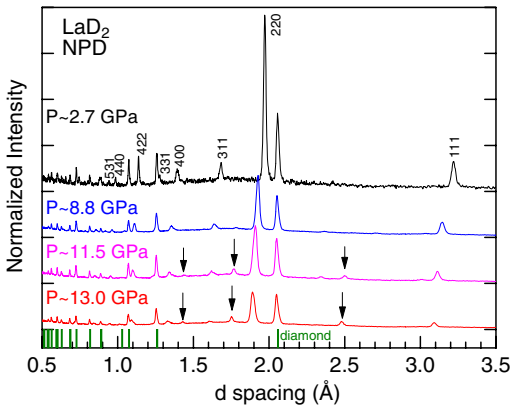

FIG. 1 (color online). Select NPD patterns measured for LaD_2 at high pressures at room temperature. Several new peaks (denoted by arrows) appear when the pressure is increased to 11.5 GPa, indicating that fcc LaD_2 decomposes into two phases. Vertical bars at the bottom show the locations of the diffraction peaks from the sintered diamond anvils.

changes in the 11.5-GPa pattern. Several peaks appear and become clearer upon increasing the pressure to 13 GPa, whereas the intensity of the original LaD_2 weakens. The locations of the new peaks agree with those of the diffraction peaks from the D-poor fcc phase observed by SR-XRD measurements.

Comparing the XRD and NPD profiles determined the occupation sites of the D atoms in the fcc metal lattice. Figure 2(a) shows the diffraction profiles obtained near 13 GPa. The contribution of the D atom with an atomic number $Z = 1$ in the XRD profile is very small compared to that of La atom with $Z = 57$; consequently, the D atom contribution can be neglected. The diffraction peaks of the D-poor phase are indexed as 111, 200, 220, 311, 222, etc., with an fcc metal lattice, $a = 4.977$ Å. The counterpart of the disproportionation products has an fct lattice, and some peaks are split into twin peaks. Deuterium in the NPD profile has a scattering length comparable to lanthanum. Hence, D and La atoms almost equally contribute to the diffraction intensity.

The NPD pattern is missing several peaks indexed with odd numbers for the D-poor phase and also $h + k + l = 4n + 2$ for the D-rich phase; these peaks are present in the XRD pattern. In the case of the D-poor phase, the lack of odd-number indexed peaks suggests a NaCl-type structure. The NaCl structure has a monodeuteride composition LaD and consists of fcc sublattices of La and D atoms off-centered along the cubic edge by half. In other words, the D atoms fully occupy the O sites of the fcc metal lattice. The missing NPD peaks have only odd indices such as 111, 311, etc. The neutron scattering lengths of La and D atoms are similar: $b_{La} = 8.24$ fm and $b_D = 6.671$ fm, respectively. For the diffractions from the fcc sublattices of La and D, the structure factor can be given by $4|b_{La} - b_D|$ for the reflections with odd indices and by

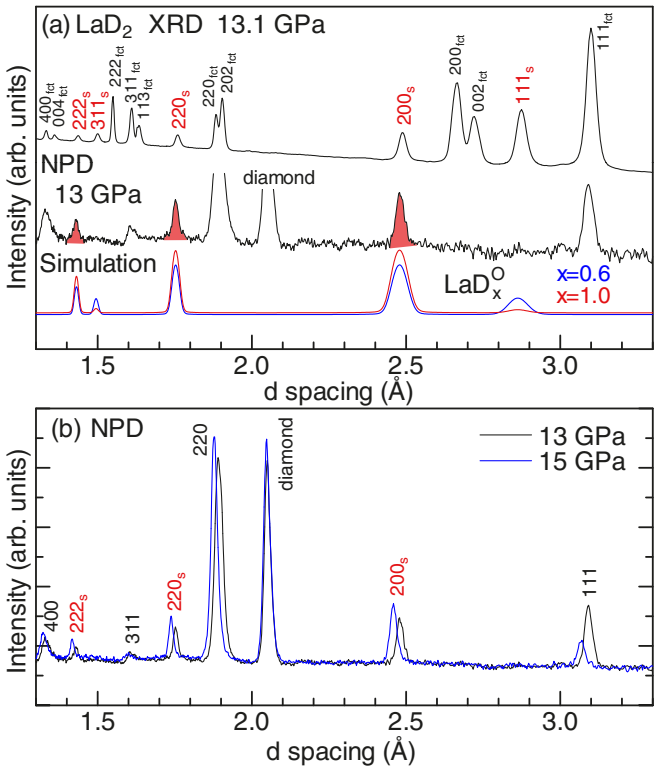

FIG. 2 (color online). (a) (top) SR-XRD, (middle) NPD profiles for the decomposed products of LaD_2 at 13 GPa, and (bottom) calculated NPD profiles for $LaD_{x<1}$. Intensities are on a logarithmic scale in arbitrary units. Solid lines at the bottom are the calculated NPD profiles for the NaCl-type structure of LaD_x with the D atoms partially ($x = 0.6$, blue line) and fully ($x = 1$, red line) occupying the O sites of the fcc metal lattice. (b) NPD patterns at 13 and 15 GPa with black and blue solid lines, respectively.

$4|b_{La} + b_D|$ for those with even indices. Thus, the close values of b_{La} and b_D yield small structure factors for the reflections of odd-number indices and consequently give small reflection intensities almost negligible. The lack of the $h + k + l = 4n + 2$ indexed peaks such as 200, 222, etc., for the D-rich phase can be explained in terms of the close b values as well.

NPD patterns are simulated for the NaCl lattice with different site occupancies of the D atom. As shown by the red solid line in the bottom of Fig. 2, full occupation of the O site or an exact NaCl structure produces satisfactory results. The disappearance of the peaks with 111 and 311 indices is consistent with the experimental results. For example, for a partial occupancy $g = 0.6$ of the O site, the 111 peak intensity returns to about one-third of the 200 peak intensity. However, a relevant peak is not observed in the NPD profile. A configuration where D atoms are distributed into both the T and O sites does not reproduce the measured pattern even with a slight partition rate of the T site. A NaCl-type structure has been reported for monohydrides of alkaline and transition metals such as LiH [28] and γ-CrH [29] but not for rare-earth metals.

Excess D atoms produced by the formation of LaD from LaD_2 likely move to the empty O sites of the mother phase LaD_2. Thus, disproportionation can be described by a reaction equation $LaD_2 \rightarrow \eta LaD + (1 - \eta)LaD_{2+\delta}$, where $2 + \delta$ represents the deuterium composition of the D-rich phase. As shown in Fig. 2(b), the 111 peak intensity of the $LaD_{2+\delta}$ phase is reduced largely with increase in pressure from 13 to 15 GPa, while the peak intensities of LaD phase slightly increase. The large reduction of the 111 peak intensity indicates an increase of the O-site occupancy of the fcc (fct) metal lattice, since the structure factor for the reflections of $LaD_{2+\delta}$ phase with odd indices is given by $4|b_{La} - g^O b_D|$ with the O-site occupancy g^O. The g^O increases gradually towards one beyond the critical value of 0.7 for the metal-insulator transition on further compression. Infrared spectroscopy measurements on $LaH_{2.3}$ confirmed the formation of insulating $LaH_{2+\delta}$ ($\delta \geq 0.7$) at pressures higher by several gigapascals above the disproportionation pressure of 11 GPa [13].

Next, we examined the thermodynamics of the disproportionation reaction and the lattice stabilities of LaH, LaH_2, and LaH_3 based on first-principles calculations. Details of the calculations are reported elsewhere [30]. Figure 3 compares the formation enthalpy of the three hydrides. The relative formation enthalpy ΔF of for the phase separation to LaH and LaH_3, with respect to the starting phase LaH_2, can be written as $\Delta F = [H(LaH) + H(LaH_3)]/2 - H(LaH_2)$, where enthalpy $H = E_0 + PV$ consists of internal energy E_0 and PV (pressure times volume). Figure 3 shows LaH_2 is energetically stable below 10 GPa but becomes unstable compared to LaH and LaH_3 at higher pressure. At ambient pressure, ΔF is approximately 0.3 eV but linearly decreases with increasing pressure and eventually becomes negative at a transition pressure of 10 GPa. Insets in Fig. 3 provide more details about the transition; each inset displays the contribution of an individual component of ΔF, internal energy ΔE_0, and

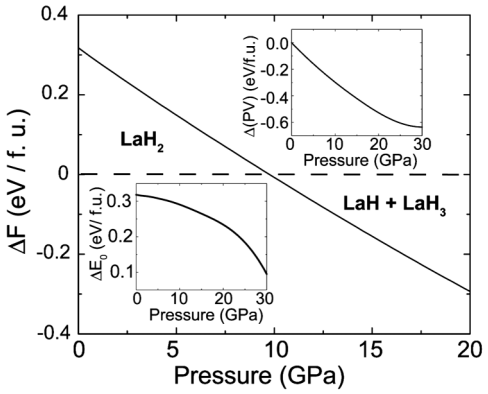

FIG. 3. Relative formation enthalpy ΔF of fcc LaH_x as a function of pressure. Insets show variations in the relative internal energy ΔE_0 (lower left) and $\Delta(PV)$ (upper right) with pressure. Spacing of pressure data points is 1 GPa or denser, and the curve is a cubic-spline fit of the calculated data points.

$\Delta(PV)$. The rapid decrease in $\Delta(PV)$ under pressure overcomes the contribution of ΔE_0, causing $\Delta F < 0$ above 10 GPa.

Dynamic stability calculations provide more information about the disproportionation. Figure 4 shows the phonon dispersion curves and the corresponding phonon density of states (PDOS) of LaH, LaH_2, and LaH_3. At low pressure (4 GPa), we determined the stabilized phonon dispersion curves by using the dynamic stability of LaH_2 [Fig. 4(b)]. Additionally, we confirmed the dynamic stability of LaH and LaH_3 at high pressure (15 GPa) [Figs. 4(a) and 4(c), respectively]. It is worth noting that LaH_2 is dynamically stable up to at least 30 GPa and LaH is stable at almost ambient pressure, indicating that LaH_2 and LaH are metastable phases above and below the transition pressure, respectively. In our decompression experiment, LaH exists down to 8 GPa where the lattice parameter is 5.03 Å. For further decompression, the diffraction peaks from LaH disappeared around 7 GPa, which shows clearly a hysteresis of the phase separation and metastability.

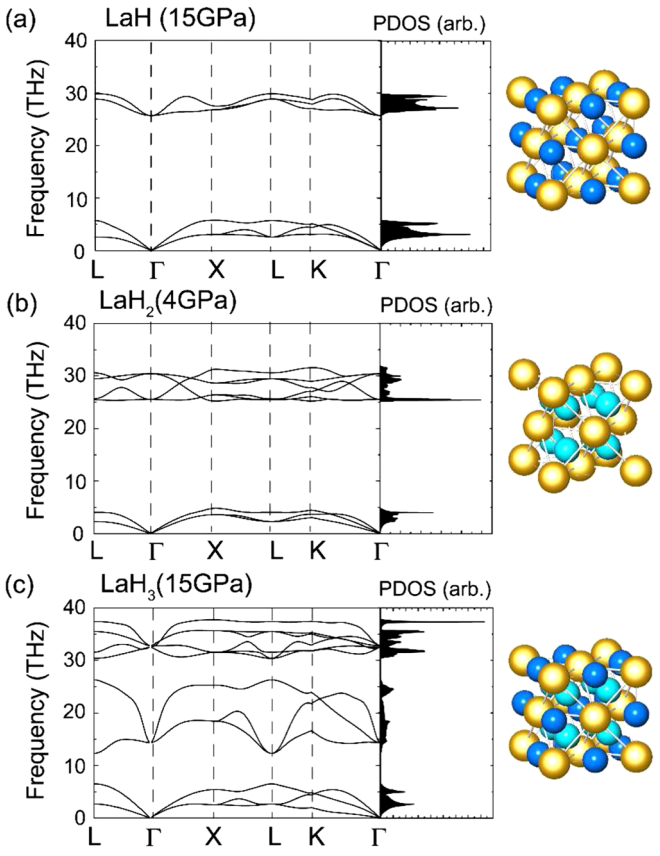

FIG. 4 (color online). Phonon dispersion curves and corresponding PDOS of (a) LaH at 15 GPa, (b) LaH_2 at 4 GPa, and (c) LaH_3 at 15 GPa. In all three panels, black solid lines show the stabilized phonon dispersion relations, and the corresponding shaded areas exhibit PDOS. Crystal structures are illustrated on the right side of each graph. Yellow, blue, and cyan spheres denote lanthanum, T-site, and O-site H atoms, respectively.

As shown in Fig. 4(a), the H atom in LaH is positioned on the O site, and the acoustic and optical branches, which represent the vibrations of La and H, respectively, are separated. This separation of the phonon vibration remains for LaH_2 where two H atoms occupy the T sites. The H^T (H atom at the T site) is the nearest neighbor of La. La and the H^T form a strong bond, which is reflected in the well-separated phonon bands of La and H^T [Fig. 4(b)], and they show phonon dispersions similar to those of LaH. However, for LaH_3, there are two distinguishable H atoms at the T and O sites, where the H^O (H atom at the O site) forms intermediate optical phonon bands [Fig. 4(c)] possessing dispersive curves in the range 10–25 THz at 15 GPa. The H^O is the next-nearest neighbor of La, and the corresponding electron transfer from La is smaller for the H^O than for the H^T, leading to the middle phonon band.

For the first time, NaCl-type monohydride LaH(D) is formed by the pressure-induced disproportionation of $LaH(D)_2$. Consistent with the experimental results, first-principles calculations indicate that the monohydride is thermodynamically and lattice dynamically stable at high pressures. The monohydride is predicted to be metastably recovered at low pressures. Similar pressure-induced reactions have been observed for YH_2, ScH_2, and NdH_2 in preliminary XRD measurements; the formation of NaCl-type monohydride is likely a common behavior for the disproportionation of rare-earth-metal dihydrides. The mono-, di-, and trihydrides having H atoms at solely the O site, solely the T sites, and both the O site and T sites, respectively, in fcc metal lattices are all present. Comparison study of their electronic states will clarify the site-dependent nature of H-M bonds in rare-earth hydrides.

The SR-XRD experiments were performed under Proposal No. 2010A3703 in BL22XU and No. 2009B3610 in BL14B1 at SPring-8. The NPD experiment was performed under the S-type neutron research project (Proposal No. 2009S06) of IMSS, KEK. This work has been partially supported by the New Energy and Industrial Technology Development Organization (NEDO) under Advanced Fundamental Research on Hydrogen Storage Materials. D. Y. K. acknowledges support by the U.S. DOE BES Grant No. DE-SG0001057.

*machida@spring8.or.jp
†Present address: National Institute for Materials Science (NIMS), 1-2-1 Sengen, Tsukuba, Ibaraki 305-0047, Japan.
‡Present address: Institute for Materials Research, Tohoku University, 2-1-1 Katahira, Sendai 980-8577, Japan.
§Present address: High Energy Accelerator Research Organization (KEK), 1-1 Oho, Tsukuba, Ibaraki 305-0801, Japan.

[1] P. Vajda, in *Handbook on the Physics and Chemistry of Rare Earths*, edited by K. A. Gschneider, Jr., and L. Eyring (Elsevier Science B. V., Amsterdam, 1995), Vol. 20, p. 207.
[2] C. E. Holley, Jr., R. N. R. Mulford, F. H. Ellinger, W. C. Koehier, and W. H. Zachariasen, J. Phys. Chem. **59**, 1226 (1955).
[3] G. Renaudin, K. Yvon, W. Wolf, and P. Herzig, J. Alloys Compd. **404–406**, 55 (2005).
[4] J. N. Huiberts, R. Griessen, J. H. Rector, R. J. Wijngaarden, J. P. Dekker, D. G. de Groot, and N. J. Koeman, Nature (London) **380**, 231 (1996).
[5] P. J. Kelly, J. P. Dekker, and R. Stumpf, Phys. Rev. Lett. **78**, 1315 (1997).
[6] K. K. Ng, F. C. Zhang, V. I. Anisimov, and T. M. Rice, Phys. Rev. Lett. **78**, 1311 (1997).
[7] R. Eder, H. F. Pen, and G. A. Sawatzky, Phys. Rev. B **56**, 10 115 (1997).
[8] T. Miyake, F. Aryasetiawan, H. Kino, and K. Terakura, Phys. Rev. B **61**, 16 491 (2000).
[9] P. van Gelderen, P. A. Bobbert, P. J. Kelly, G. Brocks, and R. Tolboom, Phys. Rev. B **66**, 075104 (2002).
[10] M. Rode, A. Borgschulte, A. Jacob, C. Stellmach, U. Barkow, and J. Schoenes, Phys. Rev. Lett. **87**, 235502 (2001).
[11] G. Schöllhammer, W. Wolf, P. Herzig, K. Yvon, and P. Vajda, J. Alloys Compd. **480**, 111 (2009).
[12] A. Machida, T. Watanuki, D. Kawana, and K. Aoki, Phys. Rev. B **83**, 054103 (2011).
[13] Y. Sakurai, A. Machida, and K. Aoki, Solid State Commun. **151**, 815 (2011).
[14] R. Oishi, M. Yonemura, Y. Nishimaki, S. Torii, A. Hoshikawa, T. Ishigaki, T. Morishima, K. Mori, and T. Kamiyama, Nucl. Instrum. Methods Phys. Res., Sect. A **600**, 94 (2009).
[15] P. Klavins, R. N. Shelton, R. G. Barnes, and B. J. Beaudry, Phys. Rev. B **29**, 5349 (1984).
[16] T. Watanuki, A. Machida, T. Ikeda, A. Ohmura, H. Kaneko, K. Aoki, T. J. Sato, and A. P. Tsai, Philos. Mag. **87**, 2905 (2007).
[17] A. Machida, T. Watanuki, A. Ohmura, T. Ikeda, K. Aoki, S. Nakano, and K. Takemura, Solid State Commun. **151**, 341 (2011).
[18] J. M. Besson, R. J. Nelmes, G. Hamel, J. S. Loveday, G. Weill, and S. Hull, Physica (Amsterdam) **180B–181B**, 907 (1992).
[19] F. Izumi and K. Momma, Solid State Phenom. **130**, 15 (2007).
[20] T. Hattori, Y. Katayama, A. Machida, T. Otomo, and K. Suzuya, J. Phys. Conf. Ser. **215**, 012024 (2010).
[21] J. P. Perdew, J. A. Chevary, S. H. Vosko, K. A. Jackson, M. R. Pederson, D. J. Singh, and C. Fiolhais, Phys. Rev. B **46**, 6671 (1992).
[22] J. P. Perdew, K. Burke, and M. Ernzerhof, Phys. Rev. Lett. **77**, 3865 (1996).
[23] P. Hohenberg and W. Kohn, Phys. Rev. **136**, B864 (1964).
[24] W. Kohn and L. J. Sham, Phys. Rev. **140**, A1133 (1965).
[25] P. Giannozzi *et al.*, J. Phys. Condens. Matter **21**, 395502 (2009); http://www.quantum-espresso.org
[26] H. J. Monkhorst and J. D. Pack, Phys. Rev. B **13**, 5188 (1976).
[27] S. Baroni, S. de Gironcoli, A. Dal Corso, and P. Giannozzi, Rev. Mod. Phys. **73**, 515 (2001).
[28] S. R. Gunn and L. G. Green, J. Am. Chem. Soc. **80**, 4782 (1958).
[29] V. E. Antonov, A. I. Beskrovnyy, V. K. Fedotov, A. S. Ivanov, S. S. Khasanov, A. I. Kolesnikov, M. K. Sakharov, I. L. Sashin, and M. Tkacz, J. Alloys Compd. **430**, 22 (2007).
[30] D. Y. Kim, R. H. Scheicher, and R. Ahuja, Phys. Rev. Lett. **103**, 077002 (2009).